On the cutting edge of semiconductor sensors: towards intelligent X-ray detectors

Bosma, M.J.

Publication date
2012

1

X-ray imaging

X-ray imaging is based on the principle of material-dependent attenuation of X-rays. The extent to which various constituents of an object, such as bone or tissue in a human body, attenuate X-rays determines the flux of photons that exit from the object. This results in an intensity distribution, which is commonly mapped by a position sensitive detector. Advanced detectors consist of a pixellated sensor and an equally dimensioned read-out chip, which digitises the image. Depending on the material used, the sensor converts X-ray quanta either directly or indirectly into an electrical signal, which is subsequently processed by read-out electronics.

This chapter gives an introduction to X-ray imaging. First, the X-ray conversion processes are discussed in terms of the most dominant interaction mechanisms and the resulting photon attenuation in the diagnostic energy domain. The efficiency of the conversion process as well as the subsequent acquisition and processing of the generated signal determines to a considerable extent how much information of the original intensity distribution is conserved in the output image. This translates into image quality discussed in Section 1.2. In this context, the detective quantum efficiency is introduced, a common figure of merit to parameterise imaging performance. Subsequently, a short history of X-ray imaging systems is given, with a particular focus on the evolution from analogue to digital detectors. The last section evaluates the flat-panel detector, today's most widely used radiography system. Its main limitations may be eliminated by a novel detector that combines high-quality sensors with intelligent read-out electronics.

1.1 X-ray interaction

1.1.1 Interaction mechanisms

X-rays interact with matter through different mechanisms, three of which are dominant in the diagnostic energy domain (∼20 - 120 keV): photoelectric absorption, Compton scattering and Rayleigh scattering. Each of them is schematically depicted in Figure 1.1.

Photoelectric absorption

Photoelectric absorption involves the absorption of an incident X-ray photon by an atomic electron[1]. This electron is ejected from its parent atom, causing ionisation. The kinetic energy transferred (E_{kin}) to the liberated electron, the photoelectron, is equal to the difference between the energy of the incident X-ray photon (E_0) and the binding energy of the electron (E_{bind}):

$$E_{\text{kin}} = E_0 - E_{\text{bind}} \,. \tag{1.1}$$

The energy of the X-ray photon must at least equal the binding energy of an atomic electron for the photoelectric ionisation to occur. Tightly bound electrons, such as K-shell electrons, have a higher binding energy than outer-shell electrons. If absorption is not possible with inner-shell electrons, interaction may occur with outer-shell electrons. The interaction probability is highest when the X-ray photon energy equals the binding energy and decreases again with higher incident energies. This sharp increase of the interaction cross-section at the binding energy is known as an edge. Logically, they are called K-edge for K-shell electrons and L-edge for L-shell electrons. Each element has its own characteristic edges. For silicon, the K-edge energy is $\sim$ 1839 eV and the L_1-shell energy is $\sim$ 149.8 eV [1]. Bone, which consists primarily of calcium, has a K-edge energy of $\sim$ 4038 eV and an L-edge energy of 438.5 eV.

Compton scattering

Compton scattering involves the incoherent scattering of an X-ray photon by an atomic electron. This interaction mainly occurs when the X-ray photon has an energy that is much higher than the binding energy of the electron. The relation between the fractional energy loss and the scattering angle θ of the photon is given by the Klein-Nishina formula [2]:

$$\frac{E_1}{E_0} = \frac{1}{1 + \alpha(1 - \cos\theta)} \,, \tag{1.2}$$

where

$$\alpha = \frac{E_0}{m_{\text{e}}c^2} \,. \tag{1.3}$$

[1] in contrast to the photoelectric effect that was discovered in 1905, which explained the ejection of electrons from the surface of crystalline structures by the absorption of visible photons.

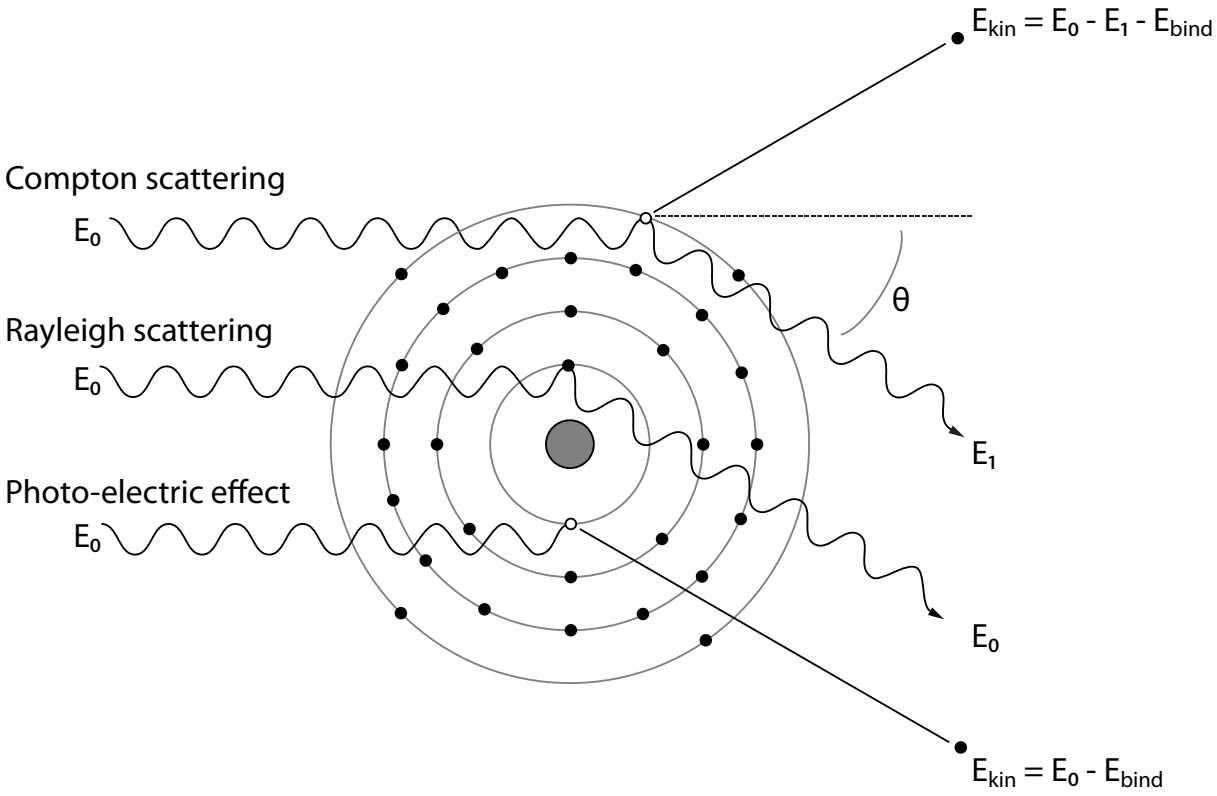

Figure 1.1: Interaction mechanisms
Schematic representation of the three interaction mechanisms in the diagnostic energy range. Whereas for both the photoelectric absorption and Compton scattering electrons are knocked out, Rayleigh scattering does not involve ionisation.

The kinetic energy of the scattered electron is equal to the difference between the initial and final photon energy minus the electron's binding energy:

$$E_{\text{kin}} = E_0 - E_1 - E_{\text{bind}} \,. \tag{1.4}$$

High-energy photons undergo small angle Compton scattering, whereas low-energy photons are more uniformly scattered.

Post-electron-ejection The vacancies left in the inner atomic shells, as a result of both photoelectric absorption and Compton scattering, are filled by outer-shell electrons. An electron of a higher atomic shell falls into the vacancy and the binding-energy difference between those shells is either emitted in the form of characteristic X-rays, also known as fluorescent X-rays, or causes ejection of Auger electrons. These are electrons from the same atom with a binding energy less than the energy released by the filling of the inner-shell vacancy. The number of fluorescent X-rays emitted per de-excitation is known as the fluorescence yield ω. Typical values for ω involving the filling of K-shell vacancies are ~ 0.05 for silicon, ~ 0.55 for gallium arsenide and ~ 0.85 for cadmium telluride [3].

Rayleigh scattering

Rayleigh scattering does not cause ionisation. Incident X-rays are coherently scattered by atomic electrons through interaction with their electric field, whereby the energy of the photons is conserved. The direction of the photons, however, is altered in this process and is quantified by the scattering angle. Similar to Compton scattering, the deflection of incident X-rays is energy dependent. Although Rayleigh scattering does not involve ionisation, it does affect image quality. Rayleigh scattering is most likely to occur at low X-ray energies in high-Z materials.

Pair creation

At higher energies, above twice the rest mass of electrons (i.e. 1022 keV), X-ray quanta can produce electron-positron pairs. Pair creation involves interaction with the electric field of the nucleus, though the atom involved is not ionised. Diagnostic energies, however, range typically from 20 to 120 keV, which is well below the pair-production threshold. Hence, pair production will not occur in medical imaging and will be ignored in this thesis.

1.1.2 Attenuation

The interaction mechanisms combine to remove X-ray photons from the incoming beam as they pass through matter. This reduction is called attenuation and involves both absorption and scattering. Attenuation is parameterised by the linear attenuation coefficient μ (cm^{-1}), which is the probability of an X-ray photon interaction per unit path length travelled through the material. This parameter can be expressed as the sum of interaction probabilities of the individual mechanisms. For the diagnostic energy regime, this is:

$$\mu = \tau + \sigma_{\mathrm{R}} + \sigma_{\mathrm{C}} \,, \tag{1.5}$$

where τ is the photoelectric interaction probability per unit length and σ_{R} and σ_{C} are the probabilities for Rayleigh and Compton scattering, respectively. Figure 1.2 shows in which energy region each mechanism is dominant for four different sensor materials. One can see that for low-Z materials, such as silicon, Compton scattering dominates when the X-ray photon energy is higher than 50 keV.

To calculate the attenuation coefficient of materials that are composed of different elements, the linear attenuation coefficient of the individual elements are commonly normalised to their density. This normalised parameter is called the mass attenuation coefficient μ/ρ (cm^2/g). Hence, following Lambert-Beer's law [4, 5], the fractional reduction of intensity (I_1/I_0) of a photon beam that passes through a slab of material is described by:

$$\frac{I_1}{I_0} = e^{-\frac{\mu}{\rho}\,\rho x} \,, \tag{1.6}$$

where x (cm) is the thickness of the material.

The individual interaction probabilities depend on the density ρ and atomic number Z of the sensor as well as the energy E of the incoming photons. For diagnostic X-rays,

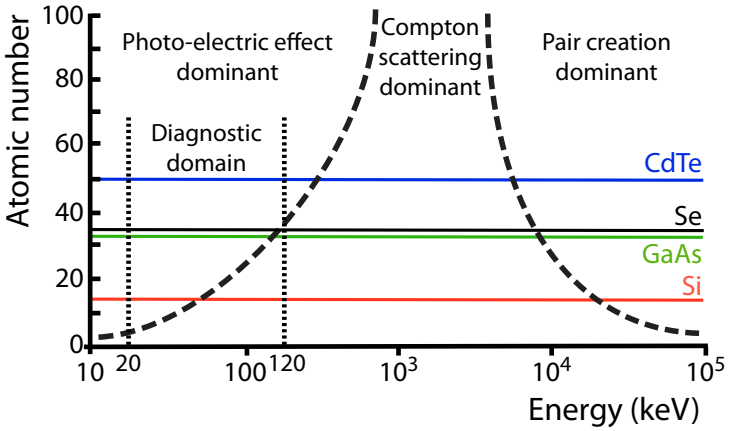

Figure 1.2: Atomic-number dependence
The energy domains in which the various X-ray interaction processes are dominant as a function of the atomic number of the absorber material. For reference, lines are drawn for the atomic numbers of silicon, gallium arsenide, selenium and cadmium telluride.

the dependencies of the photoelectric and Compton mass attenuation coefficients are approximately as follows:

$$\begin{aligned} \tau/\rho &\propto (Z^{4-5}, E^{-3}) \\ \sigma_{\mathrm{C}}/\rho &\propto (Z, E-\text{independent})\,. \end{aligned} \tag{1.7}$$

The energy dependence can be seen in Figure 1.3(a), which shows the total mass attenuation coefficient as a function of the energy of the incoming photon. The fraction by which the intensity is attenuated as a function of initial photon energy is shown in Figure 1.3(b). Curves are drawn for the sensor materials studied in this thesis and compared to that of selenium, a commonly used material in current X-ray imaging detectors.

The mass attenuation coefficient only describes the intensity reduction and does not express the amount of energy deposited in the sensor. The energy deposition is, however, important for the calculation of the signal generated. It is described by the mass energy transfer coefficient μ_{tr}/ρ (cm^2/g). It is the fraction of the mass attenuation coefficient that reflects how much of the energy of the incoming photon is transferred to kinetic energy of the photoelectron or Auger electron:

$$\frac{\mu_{\mathrm{tr}}}{\rho} = \left(\frac{E_{\mathrm{kin}}}{E_0}\right)\frac{\mu}{\rho}\,. \tag{1.8}$$

The mass energy absorption coefficient even takes radiative losses into account, but those are negligible in the diagnostic energy domain.

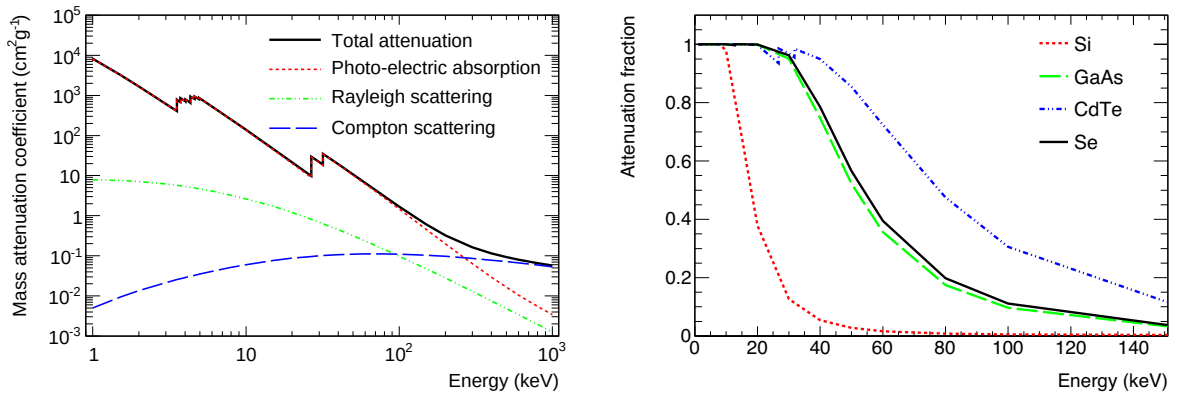

(a) (b)

Figure 1.3: Attenuation
(a) The total mass attenuation coefficient of cadmium telluride and the contributions of the different interaction mechanisms as a function of the energy of the X-ray photon. (b) The absorption efficiency as a function of photon energy for slabs of 500 µm thick silicon (Si), gallium arsenide (GaAs), cadmium telluride (CdTe) and selenium (a-Se). Based on the mass attenuation coefficients from [6].

1.2 Image quality

The main requirement for an X-ray detection system is to deliver high-quality images using the lowest possible dose. Image quality can be parameterised by the signal-to-noise ratio, which describes the extent to which a signal exceeds the background noise. However, this is only a poor descriptor, since it contains no information about how much detail can be distinguished in the image. A better figure of merit is the detective quantum efficiency [7, 8], which defines the efficiency with which X-ray quanta are used for image formation as a function of spatial frequency. It compares a detector's signal-to-noise ratio with that of the same, but ideal detector, i.e. one that does not introduce noise. Given a certain object and radiation dose, this parameter allows to compare different imaging systems.
To be able to give an exact definition of the detective quantum efficiency, the most important parameters that determine image quality are introduced. This requires a description of both signal and noise transfer in the spatial-frequency domain. These are parameterised by the modulation transfer function and the noise power spectrum, respectively.

1.2.1 Qualitative description

Image quality is determined by a detector's ability to transfer an input intensity distribution to a digital output image with minimal loss of information.
As shown in Figure 1.4, there are several detector-induced phenomena that degrade an image. The severity of these effects on the image are commonly described in terms of

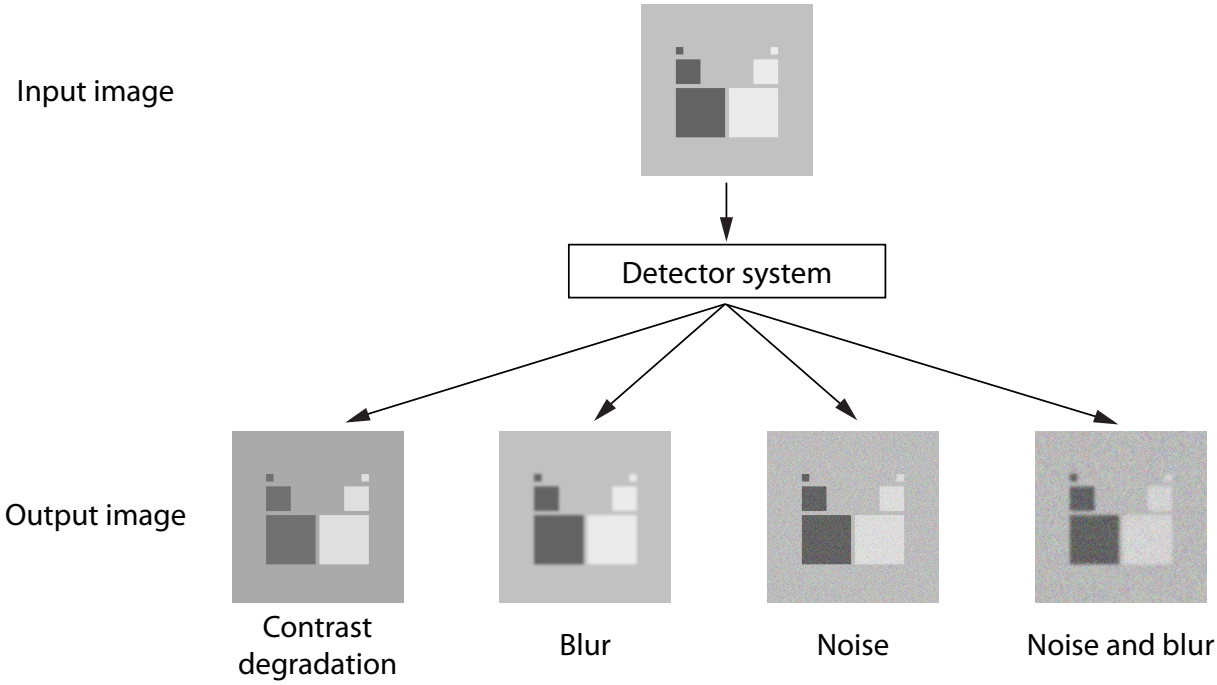

Figure 1.4: Image degradation
Image quality is determined by a detector's ability to preserve clarity of detail. The output image, however, is almost always affected by the detector. Often, a convolution of detector effects cause a degradation of the output image. Figure inspired by [9].

contrast transfer properties, spatial resolution and noise performance of the detector. The former two define image sharpness, i.e. the clarity of detail. A detector's ability to transfer contrast is parameterised by its dynamic range, determined by the bit depth of the read-out pixel (see Chapter 3). If a detector's dynamic range is insufficient, the output image will show contrast degradation with respect to the input image. Despite the fact that contrast transfer describes a detector's ability to differentiate between areas of different photon intensity, it does not express the transfer of spatial detail. This is determined by the spatial resolution of the detector, which mainly depends on the pixel size. However, several effects might compromise the position information of the incoming X-ray photon and may cause image blur. The most important effects will be evaluated in Chapter 6.
On top of contrast degradation and blur, both of which cause a reduction of image sharpness, the detector system can suffer from noise. Apart from irreducible Poisson noise due to the quantised input, the sensor and read-out electronics can introduce both stochastic and non-stochastic noise. In the rightmost image of Figure 1.4, it can be seen that noise and subsequent blur cause the smallest objects to be poorly distinguishable from their neighbouring objects. This shows that imaging performance is determined by the distance over which noise is correlated and thus demonstrates that the mean signal-to-noise ratio is only a global and hence poor descriptor of image quality.

1.2.2 The Rose model

A traditional description of signal and noise transfer is given by the Rose model [10, 11], which demonstrates that image quality is fundamentally limited by quantum statistics. The model assumes a uniform object in a uniform background and Poisson-distributed quantum noise. Consequently, the object contrast can be described by:

$$\mathrm{C_{Rose}} = \frac{(\bar{q}_b - \bar{q}_0)}{\bar{q}_b}\,, \tag{1.9}$$

with $\bar{q}_0$ representing the mean number of quanta per unit area that exits the object and $\bar{q}_b$ the mean number of background quanta per unit area ($\bar{q}_b \geq \bar{q}_0$ in the case of imaging). The signal is then defined as the difference between the number of background and object quanta integrated over the object's area A:

$$\mathrm{S_{Rose}} = A(\bar{q}_b - \bar{q}_0)\,. \tag{1.10}$$

The quantum noise is the standard deviation σ_b of the mean number of background quanta $A\bar{q}_b$, which equals to $\sqrt{A\bar{q}_b}$. In this approach, the signal-to-noise ratio as defined by Rose becomes:

$$\mathrm{SNR_{Rose}} = \frac{\mathrm{S_{Rose}}}{\sigma_b} = \frac{A(\bar{q}_b - \bar{q}_0)}{\sqrt{A\bar{q}_b}} = \mathrm{C_{Rose}}\sqrt{A\bar{q}_b}\,. \tag{1.11}$$

It shows that it is proportional to object contrast and to the square root of both the object's area and radiation dose. This demonstrates the importance of sufficient quantum statistics in image formation. The Rose model is only valid, however, for normally distributed quanta, since it does not take into account effects of spatial correlation. The image can be correlated due to scattering in the object or blur caused by the detector. To characterise these correlation effects, a Fourier-based wave approach that allows for decomposition of both signal and noise into their spatial-frequency dependent components is preferred over the uncorrelated particle approach.

1.2.3 Signal transfer

The intensity distribution at a detector's input can be seen as an ensemble of point impulses in 2D-space $\delta(x, y)$ acting on an input signal function $q(x, y)$ through integration. This function at a point (a, b) in 2D-space is then given by:

$$q(a, b) = \int_{-\infty}^{\infty}\int_{-\infty}^{\infty} q(x, y)\delta(x - a, y - b)dxdy\,. \tag{1.12}$$

Ideally, the detector's response to a point impulse is a delta function in image space. In reality, however, detector imperfections cause smearing of the input point impulse, which is parameterised by a detector's point spread function (psf). The output $d(x, y)$ is therefore expressed as a function of the input function and the point spread function:

$$d(x, y) = \int_{-\infty}^{\infty}\int_{-\infty}^{\infty} q(a, b)\mathrm{psf}(x - a, y - b)dadb\,, \tag{1.13}$$

or as the convolution of the input function with the point spread function:

$$d(x, y) = (q \otimes \mathrm{psf})(x, y)\,. \tag{1.14}$$

The output function is only representative for the entire detector if its response to a given input is both linear and shift invariant (i.e. position independent) [12]. Both linearity and shift-invariance make that the system's response to an ensemble of scaled and shifted point impulses is identical to the sum of separate responses to each of the individual point impulses and therefore allows for signal decomposition. A natural way to do this is to treat the individual signal components as single-frequency sinusoids rather than point impulses, as the output components are then eigenfunctions of their input counterparts. Since the convolution theorem states that the Fourier transform of a convolution equals the product of the individual Fourier transforms, the output as a function of spatial frequency $D(u, v)$ can be described by the product of the Fourier-transformed input function $Q(u, v)$ and the Fourier-transformed point spread function, the optical transfer function $\mathrm{OTF}(u, v)$:

$$D(u, v) = Q(u, v) \cdot \mathrm{OTF}(u, v)\,. \tag{1.15}$$

From this, it can be seen that the input function remains unchanged apart from scaling by the optical transfer function. The optical transfer function consists of a real and imaginary part: the modulation transfer function and the phase transfer function. For a shift-invariant detector, the phase transfer function equals zero and only the modulation transfer function matters.

Modulation transfer function

Clarity of detail is parameterised by the sharpness of an image. This is determined by the level of contrast as well as the spatial resolution. Both parameters are combined into one figure of merit, known as the modulation transfer function. It describes the magnitude of contrast transfer as a function of spatial frequency. Theoretically, it can be derived by considering the transfer of a sinusoidal signal using Fourier decomposition [9].
For an input signal of the following form:

$$q(x, y) = A + Be^{i2\pi(ux+vy)}\,, \tag{1.16}$$

the input modulation M_q is given by:

$$M_q = \frac{B}{A}\,. \tag{1.17}$$

Subsequently, the output $d(x, y)$ of a linear and shift-invariant system can be derived as follows:

$$\begin{aligned} d(x,y) &= \int_{-\infty}^{\infty}\int_{-\infty}^{\infty} \left(A + Be^{i2\pi(ua+vb)}\right) \mathrm{psf}(x-a, y-b)dadb \\ &= \int_{-\infty}^{\infty}\int_{-\infty}^{\infty} \left(A + Be^{i2\pi(u(x-a)+v(y-b))}\right) \mathrm{psf}(a,b)dadb \\ &= \left(A + Be^{i2\pi(ux+vy)}\right) \left[\int_{-\infty}^{\infty}\int_{-\infty}^{\infty} e^{-i2\pi(ua+vb)}\mathrm{psf}(a,b)dadb\right] \\ &= \left(A + Be^{i2\pi(ux+vy)}\right) \cdot \mathrm{OTF}(u,v) \\ &= A \cdot \mathrm{OTF}(u,v)|_{u,v=0} + B \cdot \mathrm{OTF}(u,v)e^{i2\pi(ux+vy)}\,. \end{aligned} \tag{1.18}$$

This results in an input-modulation dependent output modulation M_d:

$$M_d = \frac{B}{A}\frac{|\mathrm{OTF}(u,v)|}{\mathrm{OTF}(0,0)} = M_q\frac{|\mathrm{OTF}(u,v)|}{\mathrm{OTF}(0,0)}\,. \tag{1.19}$$

The modulation transfer function (MTF) is then defined as the ratio between output and input modulation:

$$\mathrm{MTF} = \frac{M_d}{M_q} = \frac{|\mathrm{OTF}(u,v)|}{\mathrm{OTF}(0,0)}\,. \tag{1.20}$$

It can be seen as the magnitude of the optical transfer function at a certain frequency with respect to the optical transfer function at zero frequency. The latter is known as the detector's quantum efficiency, which expresses the ratio between the mean number of recorded photons and the actual mean number of input photons.
In other words, the modulation transfer function is a factor that scales the input modulation and equals to unity at zero frequency.

1.2.4 Noise transfer

In addition to the variance in the number of Poisson-distributed input quanta, imaging systems introduce noise to the image. Typical sources are read-out noise, intensity fluctuations of the photon beam, dark currents in the sensor and detector-response variations, known as structured or fixed-pattern noise (see Chapter 6).
All cause unwanted fluctuations of the signal, which can mask the variation of the actual signal. The power of the total of these fluctuations determines the extent to which it over-shadows the signal, which is described by the power signal-to-noise ratio for normally distributed quanta. This parameter, however, does not describe the spatial-frequency content of the noise. This is represented by the noise power spectrum (NPS), which is defined as the Fourier transform of the auto-correlation function of the noise and can be experimentally obtained by determining the ensemble average of the squared magnitude of the discrete Fourier transform of the signal fluctuations. In the two-dimensional case, it can be expressed as:

$$\mathrm{NPS}_d(u,v) = \lim_{N_x,N_y,M\to\infty} \frac{\Delta x\Delta y}{MN_xN_y}\sum_{m=1}^{M}\left|\sum_{i=1}^{N_x}\sum_{j=1}^{N_y}\Delta d(x_i,y_j)e^{-i2\pi(ux_i+vy_j)}\right|^2\,, \tag{1.21}$$

where $\Delta x \Delta y$ is the pixel area, M the number of images in the ensemble, $N_x N_y$ the number of pixels that form the region of interest and $\Delta d(x, y)$ denotes the deviation from the mean signal. More detailed information on the experimental determination of the noise power spectrum is given in Chapter 6.

1.2.5 Detective quantum efficiency

Given a modulation transfer function and noise power spectrum, the detector's signal-to-noise performance can be parameterised on an absolute scale by the noise-equivalent number of quanta (NEQ) as a function of spatial frequency:

$$\mathrm{NEQ}(\bar{q}; u, v) = \frac{\bar{q}^2 \bar{G}^2 \mathrm{MTF}^2(u, v)}{\mathrm{NPS}_d(u, v)} = \frac{\bar{d}^2 \mathrm{MTF}^2(u, v)}{\mathrm{NPS}_d(u, v)}\,, \tag{1.22}$$

where $\bar{q}$ is the mean number of input quanta per unit area, $\bar{G}$ is the quantum efficiency, which describes the ratio between $\bar{q}$ and the mean number of output quanta $\bar{d}$. The noise-equivalent number of quanta expresses image noise as the apparent number of input quanta needed for image formation if the detector would only be limited by Poisson noise. In other words, it tells how many input quanta an image is worth.
It is only dependent on $\bar{d}$, the modulation transfer function and the output noise power spectrum, all of which can be obtained from image data.

An overall figure of merit for the imaging performance of the detector system is given by the ratio between the noise-equivalent number of quanta and the mean number of photons used to form the image. This parameter is called the detective quantum efficiency (DQE) and expresses the efficiency with which the input quanta are used to produce the output image:

$$\mathrm{DQE}(u, v) = \frac{\mathrm{NEQ}(u, v)}{\bar{q}} = \frac{\bar{d}^2 \mathrm{MTF}^2(u, v)}{\bar{q} \mathrm{NPS}_d(u, v)}\,. \tag{1.23}$$

For the special case, in which the input and output quanta are Poisson-noise limited, i.e. there is no spatial correlation and thus no frequency dependence, the NEQ equals $\mathrm{SNR}^2_{\mathrm{out}}$ and $\mathrm{SNR}^2_{\mathrm{in}}$ equals $\bar{q}$. This simplifies the expression for the detective quantum efficiency to:

$$\mathrm{DQE} = \frac{\mathrm{SNR}^2_{\mathrm{out}}}{\mathrm{SNR}^2_{\mathrm{in}}}\,. \tag{1.24}$$

1.2.6 Sampling

One of the difficulties in measuring the DQE of digital detectors arises from the sampling of the input image due to the pixel segmentation [13]. Sampling itself is not harmful, as it only causes the Fourier transform of the input to replicate at fixed multitudes of the sampling interval. Under-sampling, though, which is the case for almost all digital imaging systems, causes overlap of the Fourier spectra near the Nyquist frequency, which is defined as $1/2b$ with b being the sampling interval, i.e. the pixel pitch.

That is the reason why the optical transfer function is generally divided into a pre-sampling stage and a digital stage. The pre-sampling optical transfer function $\mathrm{OTF}_{\mathrm{pre}}$ describes the system's response up to the stage of sampling and contains contributions from blur inferred by the sensor and includes a pixel aperture function, which describes the shape and size of the pixel's effective active area. The digital optical transfer function $\mathrm{OTF}_{\mathrm{d}}$ is defined as the Fourier convolution of the $\mathrm{OTF}_{\mathrm{pre}}$ with a comb function $\mathrm{OTF}_{\mathrm{comb}}$, which represents the pixel sampling:

$$\mathrm{OTF}_{\mathrm{d}} = \mathrm{OTF}_{\mathrm{pre}} \otimes \mathrm{OTF}_{\mathrm{comb}} \,. \tag{1.25}$$

As a consequence of under-sampling, frequency components above the Nyquist frequency show up as low-frequency aliases in the digital MTF. As a result, the digital MTF has additional contributions from the aliased components and therefore does not describe the frequency response of a single sinusoidal input. This complicates the interpretation of the digital MTF and therefore compromises its meaning as a measure of signal-transfer performance.

Under-sampling poses a further difficulty to the experimental determination of the MTF, as it makes the detector's response phase-dependent with respect to the sampling comb and thus not shift invariant at the sub-pixel level. A way to avoid the effects of aliasing and phase dependence is to over-sample the system, which enables measurement of the response to the impulse function for all phases relative to the sampling comb. This gives the pre-sampling MTF, which can be seen as the frequency response to single sinusoidal inputs. A method to obtain the digital MTF is to mathematically derive its expectation value from the measured pre-sampling MTF. It is equivalent to averaging the digital MTF over one sampling period, i.e. pixel pitch. This parameter is known as the expectation MTF (EMTF).

1.3 Radiography detectors

Since the early fifties of the last century, X-ray imaging detectors have undergone a large and rapid development. Efforts have been made to increase image quality, to reduce the dose and to make systems more convenient to use. In the 1970s, the first computerised systems were developed. In particular, these systems were faster and cheaper to use, yet analogue systems are still widely used nowadays.
A comparison of different systems, which all have been part of the evolution of the analogue film-screen detector to the currently state-of-the-art flat-panel detector, is given below. Specifically, common features and limitations of each of the detectors will be discussed.

1.3.1 Analogue systems

Analogue radiography systems take X-ray images with a cassette which contains a film that is mounted in contact with one or two intensifying phosphor screens to increase the quantum efficiency. The screen absorbs X-rays and converts them into visible photons, which subsequently expose the film.
An important benefit of film-screen technology is the intrinsic high spatial resolution of the film. Typical grain sizes vary between 10 and 30 µm. The film's response, however, is non-linear and its dynamic range is limited, thereby reducing contrast. Moreover, analogue imaging is both space and time consuming. Film needs to be developed and the pictures require physical storage space. If the radiograph is of unsatisfactory quality, for example when it is under- or over-exposed, the entire process has to be repeated. An increase in number of retakes means an unwanted increase in dose.

1.3.2 Digital systems

Some of the shortcomings of analogue systems are eliminated by digital systems [14]. In general, digital systems have a larger and sometimes adaptive dynamic range and show a linear response, while having similar spatial resolution. This results in a better signal-to-noise ratio, as a result of which the ability to detect low-contrast structures is improved. In addition, they provide a digital output image, which allows for enhancement using digital image-processing techniques and provides the possibility of a computer-aided diagnosis. This translates to a reduction of the number of possible retakes. The increased sensitivity as well as the digitisation of images therefore reduce the average dose for the patient. Moreover, they provide the possibility of immediate image preview, which gives the opportunity to do real-time imaging.
Digital detectors can be categorised into computed-radiography systems and digital-radiography systems. In analogy to film-screen detectors, computed radiography is based on the formation of a latent image which is subsequently read out and processed to obtain the final output image. The difference is that it generates a digital image instead of an analogue print. In digital radiography detectors, on the other hand, the read-out stage is integrated in the system.
In addition, digital systems can be divided into indirect and direct conversion detectors. Direct detectors convert the X-ray photons directly to charge, providing the electrical signal. Indirect conversion means there is an intermediate stage at which X-rays are first converted to visible photons before the final conversion to charge.

Indirect conversion detectors

Two commonly used indirect conversion detectors are storage-phosphor plates and image-intensifier screens.

Storage-phosphor plates Storage-phosphor plates fall under the category of computed-radiography systems. They consist of a photostimulable plate, which stores a latent image of the object as a distribution of charges. This latent image is formed by electrons and

holes that are liberated by the X-ray photon and subsequently trapped in the plate. The resulting charge distribution is read out by exciting these charges locally by using laser light. The subsequent de-excitation causes emission of phosphorescent light, which is detected and converted to an electrical signal by a photomultiplier. The output of the photomultiplier is then digitised and displayed by a computer. The typical read-out time is of the order of one minute.

Image-intensifier screens Image-intensifier screens convert X-ray distributions to intensified visible images, which are the result of a multi-conversion and focussing process. The detector typically consists of an input and an output phosphor screen. The input screen first converts the X-ray quanta to light. The visible photons then liberate photoelectrons from a photocathode at the back of the input screen. These are accelerated and focussed onto an output phosphor screen, which converts the condensed photoelectron image to an intensified visible-photon image. Subsequently, this image is recorded by an optically coupled video camera or CCD, the electrical output of which is digitised and sent to a computer. As the read-out is integrated in the detector system, image intensifiers are classified as digital radiography detectors.

Although both detectors have the advantages of image digitisation as listed in the section 1.3.1, they possess some intrinsic limitations:

- Indirect conversion involves processes, such as light scatter in a phosphor screen, that cause lateral spread of information carriers and hence lead to a loss of resolution.
- Poor optical coupling to the photomultiplier, video camera or CCD reduces the number of information carriers and hence lowers the sensitivity. Also, it can introduce secondary quantum noise.
- Some excited states in the phosphor can be meta-stable. This causes a delayed relaxation and hence delayed phosphorescence, also known as after-glow. This makes these detectors slow and therefore unattractive for real-time imaging applications.
- Due to the separate read-out of photostimulable phosphors and the bulky parts of intensifier screen, they are space consuming.

Direct conversion detectors

The most widely used radiography system today is the flat-panel detector [15, 16].

Flat-panel detectors Flat-panel detectors consist of a so called active-matrix array of thin-film transistors (TFTs) that reads out a directly or indirectly converting layer of sensor material. Flat-panel technology allows for fabricating electronic circuits over glass substrates of large area and hence gives access to human digital radiography. Besides, these detectors are more compact than image intensifiers, as the read-out electronics form an integral part of the detector.

The read-out is realised by a patterned film of hydrogenated amorphous silicon deposited on a glass substrate, segmented into pixels. Each pixel contains a sensing electrode, a storage capacitor and a switching TFT. The charge created in the sensor is collected at the electrodes and stored on the capacitors. Subsequently, each capacitor is read out by addressing the switching TFTs in a row-wise manner [17, 18]. This way of signal processing makes that flat-panel detectors are denoted as charge integrators. That is to say, each capacitor integrates charge proportional to the amount of energy deposition in each pixel, which is determined by the number and energy of the incoming photons during a given acquisition time. Due to both the fact that the intensity of low-energy photons is attenuated more than that of high-energy photons and low-energy photons generate less charge in the sensor, the quantum noise contribution of low-energy photons is relatively high. The opposite is true for high-energy photons. Consequently, high-energy photons are given a higher weight than low-energy ones, at the expense of the signal-to-noise ratio. The output image will therefore not perfectly correspond to the attenuation profile of the object.

Typically, the sensor is a directly converting photoconductive layer of amorphous selenium (of typically 1 mm thickness) or an indirectly converting caesium iodide scintillator (of ~ 0.5 mm) on top of an active matrix of amorphous silicon photosensors [19]. As this thesis focusses on directly converting crystalline semiconductor sensors, photoconductive amorphous selenium will be used as a reference sensor material.
An intrinsic property of photoconductors is direct conversion of X-rays into charge. As a result, lateral spread of information carriers due to multiple conversion is avoided. Nonetheless, there are some shortcomings of amorphous selenium as a sensor material. First, the atomic number of selenium as well as its charge-carrier mobility is moderate. The intensity of 70 keV photons (typically used for chest radiography) is only reduced by 28 % in 0.5 mm thick selenium (see Figure 1.3(b) on page 8). To stop a substantial amount of these photons, the sensor has to be at least twice as thick. The mean drift length of both holes and electrons, however, is only of the order of 1 mm for an electric field of 10 ^{5}V/cm. As a result of the moderate carrier transport properties, the number of electron-hole pairs contributing to the signal is low. Depending on the operation voltage, the effective energy to create one electron-hole pair is between 20 and 50 eV. The resulting low quantum efficiency requires long acquisition times. Consequently, even though flat-panel detectors can provide immediate image preview, the maximum frame-rate is limited to approximately 15 frames per second for $(200\ \mu\text{m})^2$ pixels.
Moreover, selenium sensors can only operate reliably in a narrow temperature domain. Ideally, they are operated within a temperature regime between 5°C and 30°C to avoid degradation of the selenium layer. This means that the temperature has to be controlled, which makes the system more complex.

Future detectors

Flat-panel technology enables fabrication of detectors that meet many of the requirements for human X-ray imaging systems. However, as discussed above, there is room for improvement. The ideal radiography detector should provide the same or even better image quality using a lower dose. This translates into stringent detector requirements.
This thesis presents an alternative detector that combines a photon-counting chip with energy-resolving capabilities (the Medipix-3 chip) with a crystalline semiconductor sensor of high atomic number. The chip allows for correction of the energy dependence of the intensity attenuation through the object and hence provides images that are intrinsically in better agreement with the intensity distribution at the input than ones made with charge integrating detectors. Moreover, crystalline high-Z semiconductor sensors provide a high quantum efficiency due to their high absorption efficiency for diagnostic X-rays, convert X-ray directly into charge and possess good charge-transport properties.
However, the active area of the Medipix chip (~ 2 cm^2) as well as the limited area of the currently available crystals (~ 10 cm^2) form a real challenge to make competitive large area diagnostic systems. Hence, enlargement of the active area is imperative. A solution is to realise a tessellation of Medipix detectors.
The potential of such a tessellation will be explored in this thesis. In particular, the study focusses on the tile-ability of different types of edgeless sensors by examining their performance at the edge.
Before the results are presented in Chapters 4 to 6, Chapters 2 and 3 will introduce the principles, operation and fabrication of crystalline semiconductor sensors as well as the Medipix detector, respectively.